Applied Physics Express **11**, 012001 (2018)
https://doi.org/**10.7567/APEX.11.012001**

UV plasmonic device for sensing ethanol and acetone

Mitsuhiro Honda[1,2*], Yo Ichikawa[1], Alex G. Rozhin[3], and Sergei A. Kulinich[2]

[1]*Graduate School of Engineering, Nagoya Institute of Technology, Nagoya 466-8555, Japan*
[2]*Institute of Innovative Science and Technology, Tokai University, Hiratsuka, Kanagawa 259-1292, Japan*
[3]*Aston Institute of Photonic Technologies, Aston University, Birmingham B4 7ET, U.K.*

*E-mail: honda.mitsuhiro@nitech.ac.jp

Received October 25, 2017; accepted November 14, 2017; published online December 1, 2017

In the present study, we demonstrate efficient detection of volatile organic vapors with improved sensitivity, exploiting the localized surface plasmon resonance of indium nanograins in the UV range (UV-LSPR). The sensitivity of deep-UV-LSPR measurements toward ethanol was observed to be 0.004 nm/ppm, which is 10 times higher than that of a previously reported visible-LSPR device based on Ag nanoprisms [Sensors **11**, 8643 (2011)]. Although practical issues such as improving detection limits are still remaining, the results of the present study suggest that the new approach based on UV-LSPR may open new avenues to the detection of organic molecules in solid, liquid, and gas phases using plasmonic sensors.

Plasmonic phenomena have greatly contributed to nanooptics and nanophotonics owing to their features such as light localization and high sensitivity to the surrounding environment.[1–3] The first application of surface plasmon resonance (SPR) for gas and biosensing reported in 1983[4] led to advances in the optical detection of chemical and biological analytes, also stimulating subsequent applications of SPR to environmental monitoring and medical diagnostics.[5–8] The recent progress in material fabrication techniques allowed for nanoparticles (NPs) exhibiting localized surface plasmon resonance (LSPR), which additionally offers the tunability of LSPR wavelength and small sensing volumes.[9] Using the LSPR of noble metal nanostructures, vapors of several inorganic and organic molecules were detected, typically at levels of 1–10 vol %.[10–15] Although gold and silver, which demonstrate plasmonic properties in visible to near-IR regions, are utilized as the most common sensing platforms, the use of other metals is believed potentially to extend the range of target molecules and reduce sensor costs, as well as detection limits. Some candidates for such metals might be Al or In, whose NPs exhibit plasmonic properties in the UV range (240–350 nm) where many organic molecules absorb light. This idea has recently been confirmed and utilized in spectroscopy and UV photocatalysis.[16–20] Very recently, Tanabe et al. systematically studied SPR wavelength shifts of thin Al films in the range from far UV to deep UV (120–300 nm) and suggested a UV-SPR-based sensor that depends on refractive index changes.[21]

In this work, for the first time, we demonstrate LSPR-based gas sensing realized in the UV range. As proof of the concept, the LSPR response of indium-based UV plasmonic nanostructures to ethanol and acetone was studied at different wavelengths. It was found that the deep-UV LSPR was more sensitive to ethanol vapor than the near-UV LSPR. The detection limits exhibited by our UV-LSPR gas sensing device were ~500 and ~1500 ppm for ethanol and acetone, respectively. Both the sensitivity and detection limit observed in this study are about 10 times greater than those previously reported by Ma et al. for Ag NPs.[15]

As the UV plasmonic device, granular In films were formed on quartz substrates by the thermal evaporation of an indium wire (99.999% purity, Nilaco) in vacuum (~10^{-3} Pa). The evaporation rate was controlled at 0.05 nm/s by monitoring using a quartz crystal microbalance. Both the film thickness and the substrate tilting angle were varied to control the film morphology and, consequently, the plasmon resonance properties of the produced In grains within the UV range. The real-time LSPR spectral response to ethanol (and acetone) was measured with the custom-made setup presented schematically in Fig. 1. The white light radiated by deuterium and halogen lamps was guided through an optical fiber to illuminate the In device fixed in a chamber. The transmitted light was collected by another fiber and extinction spectra were measured using a spectrometer (Tokyo Instruments Silver Nova) with a wavelength resolution of ~1 nm. The exposure time for one spectrum was 1.5 s, while a series of spectra were measured in gas flow at intervals of 2.5 s. To show changes in LSPR wavelength shift over time, each spectrum was analyzed by curve-fitting using a single Gauss function to obtain the precise peak position. Gases with defined concentrations were prepared by vaporizing the corresponding liquids under N_2 flow at 27 °C, their concentrations being confirmed using standard indicator tubes. The concentration of ethanol was varied from 500 to 10,000 ppm (1%), while that of acetone was less than 1,500 or 4,000 ppm (for different devices), the latter concentration being explained by the interference of UV light absorption peaks of acetone that restricted LSPR measurements at higher concentrations.

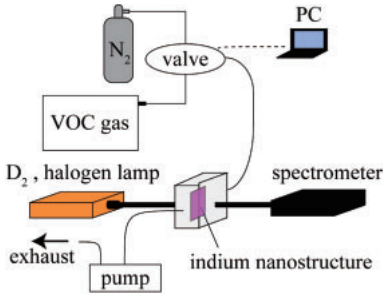

Fig. 1. Schematic illustration of setup for gas sensing based on UV plasmonic properties of In nanostructures.

Figure 2 presents atomic force microscopy (AFM) surface images of four In nanostructures prepared and tested in this study. The samples were deposited at different substrate angles and with different thicknesses; such parameters are presented in Table I. Samples 1, 2, and 3 were prepared with thicknesses of 10, 15, and 20 nm [see Figs. 2(a)–2(c)], respectively, whereas sample 4 was fabricated with a thickness of 25 nm at a substrate tilting angle of ~85° [Fig. 2(d)]. The

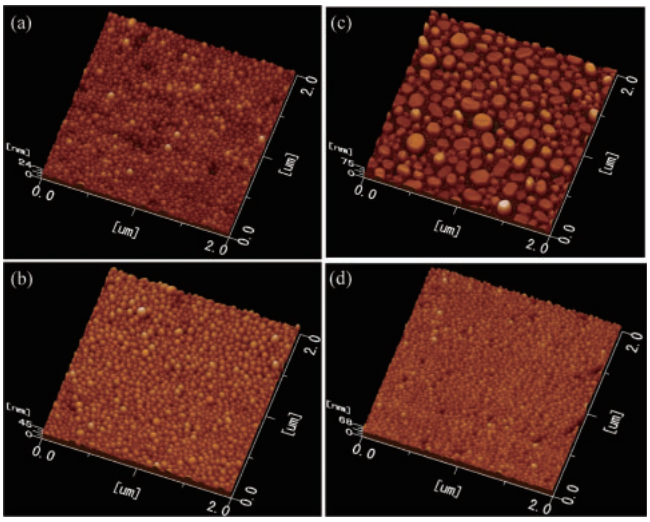

Fig. 2. AFM surface images of In grains prepared as samples 1 (a), 2 (b), 3 (c), and 4 (d). The deposition thicknesses were 10 (a), 15 (b), and 20 nm (c). The sample in panel (d) was deposited at a tilt angle of 85° and was 25 nm thick.

Table I. Thickness and grain size evaluated by AFM, LSPR wavelength from extinction spectra, and substrate angle during preparation of samples used in this study.

	Sample No.			
	1	2	3	4
Substrate angle (°)		0		85
Deposition thickness (nm)	10	15	20	25
Lateral size (nm)	30	60	86	24
Height (nm)	5	18	34	11
LSPR wavelength (nm)	295	316	322	270

grain size is seen to increase with the sample thickness in Figs. 2(a)–2(c) and Table I. The lateral size and height of the prepared grains were found to change from 30 to 86 nm and from 5 to 34 nm, respectively, as the samples were deposited for longer times (see Table I). A comparison between surface images in panels (c) and (d) indicates that sample deposition on a tilted substrate provided In grains with different aspect ratios. More specifically, hemispherical In grains (the ratio of their lateral size to height was ~1/2) were prepared in sample 4. This observation is in good agreement with those in previous studies by other researchers who also considered deposition on a tilted substrate (the so-called "oblique angle deposition").[22,23] Thus, sample 4 had In nanograins with a drastically different morphology.

Figure 3 shows extinction spectra of the samples previously described in Table I and Fig. 2. Black, green, and blue spectra represent the extinction of samples 1, 2, and 3, whose surface images are given in Figs. 2(a)–2(c), respectively. The LSPR wavelength is clearly observed to shift toward smaller values in thinner samples, which is attributed to the size reduction of In grains. Thus, varying the deposition thickness allowed us to control the LSPR wavelength within the near-UV range. The red spectrum belongs to sample 4, whose peak wavelength is seen to shift to values as small as 270 nm. This is believed to result from the different morphology achieved in this sample (hemispherical grains with a height/diameter ratio of 1/2). Previously, LSPR wavelength shifts

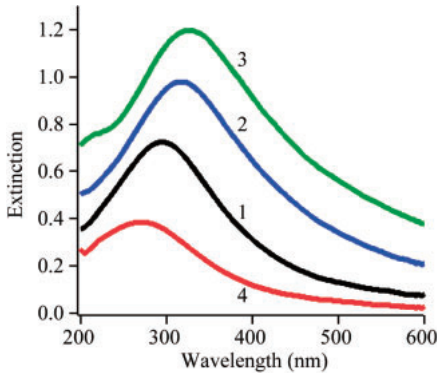

Fig. 3. Extinction spectra of samples 1 (black), 2 (blue), 3 (green), and 4 (red).

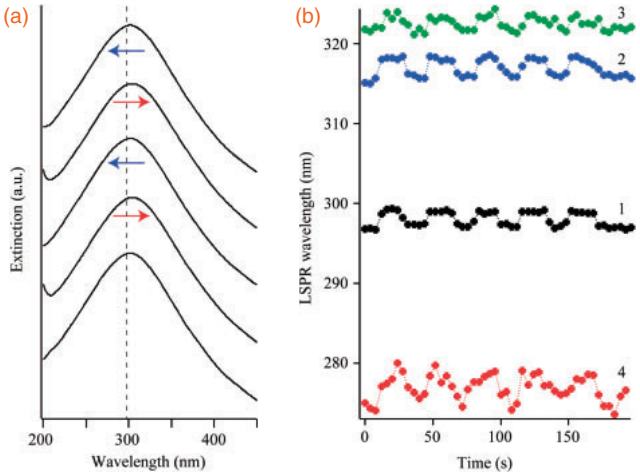

Fig. 4. (a) Extinction spectra of sample 1 measured during alternate injection of ethanol (1%) or pure N_2. Red and blue arrows indicate alternate LSPR shifts due to ethanol and N_2 gas injections, respectively. (b) LSPR responses of samples 1, 2, and 3 (black, blue, green lines), and that of sample 4 (red line) to ethanol (1%) flow.

caused by changes in Ag NP height were reported.[24] It should be noted that the Mie theory also supports shorter LSPR wavelengths in oblate ellipsoid structures with smaller aspect ratios.[25] In this study, the LSPR wavelength of the prepared nanostructures was expanded to the deep-UV range where many biological molecules efficiently absorb light, which makes the present results potentially applicable to bioimaging and related applications.

All the above-described samples were tested as ethanol gas sensing devices. Figure 4(a) presents the extinction spectra of sample 1 during the alternate injection of ethanol and nitrogen gases at controlled flow rates (~1.5 L/min). The ethanol concentration used in this experiment was 1 vol% (10,000 ppm). The LSPR wavelength is seen, in Fig. 4(a), to red- or blue-shift in response to either ethanol or pure N_2 gas, respectively. A similar redshift of LSPR wavelengths was previously reported by Anker et al. for plasmonic NPs placed in solvents with higher refractive indices.[2] Since the absorption band of ethanol is not in the range of 200–400 nm, the spectral shift observed in Fig. 4(a) is concluded to result from refractive index changes at the NP/adsorbed gas molecule interface.

Figure 4(b) shows temporal changes in LSPR wavelengths of all four samples as they were exposed alternately to ethanol

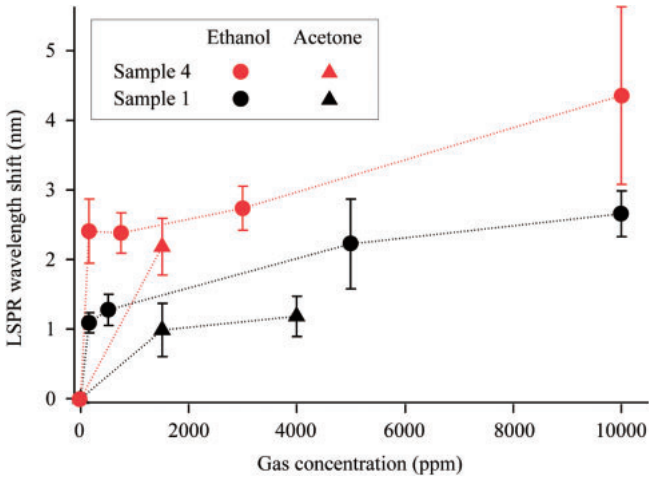

Fig. 5. Sensitivities to ethanol (circles) and acetone (triangles) versus gas concentration demonstrated by samples 4 (red) and 1 (black). Lines are given as visual guides only.

and nitrogen flow. Black, blue, green, and red colors indicate samples 1, 2, 3, and 4, respectively. Note that the black line here corresponds to the peak position shifts observed in Fig. 4(a). It is clearly observed that all the samples responded to ethanol as their LSPR wavelength positions periodically changed within ~4 s when their gas environment changed. This implies that the LSPR response of the prepared nanostructures to ethanol was reversible and fast, being attributed to the physisorption of gas molecules on the NP surface.

The response demonstrated by sample 4 [red line in Fig. 4(b)] is seen to be incomplete and slower, with more fluctuations and incomplete recovery to the initial state. This is probably caused by ethanol adsorbed between grains. As seen in the AFM image [Fig. 2(d)], In grains are closely packed on this sample surface. As a result, ethanol absorbed (and probably even condensed as liquid droplets) inside such intergranular trenches could not be eliminated quickly with nitrogen gas flow, which is why no highly reproducible response was recorded with this sample. This assumption is supported by Fig. 5, where one can see that at lower ethanol concentrations (3,000 ppm and less), when no liquid droplets were expected to form in the intergranular space of the surface, a much more stable and reproducible signal was observed with sample 4 (red circles in Fig. 5).

It is clearly seen in Fig. 4(b) that the spectral shift observed in response to ethanol injection or removal depends on the sample morphology (or more specifically, on the grain size and density on the sample surface). Sample 4 [red line in Fig. 4(b)], whose LSPR wavelength is observed at 270 nm, is seen to demonstrate the largest shifts. The refractive index at the ethanol/NP interface should increase at wavelengths close to the absorption band of ethanol, which is expected to result in more significant modulations of LSPR. Zhao et al. reported similar results for Ag NPs in the visible range when LSPR demonstrated more pronounced shifts at wavelengths close to those where target gas molecules absorb.[9] In Fig. 4(b), however, the modulations observed for sample 1 (black) are smaller than those for sample 2 (blue). As shown in Table I, In grains in sample 1 have a very fine structure (on the order of 5 nm) and, since the sample surface is expected to be covered by an oxide layer, typically <4 nm thick,[26] the gap between the metallic surface and surrounding ethanol molecules can be as large as ~10 nm. This may explain why a weaker LSPR response was demonstrated by sample 1, even though its LSPR wavelength is relatively short (~295 nm). Apart from this finding for sample 1, Fig. 4(b) demonstrates that, owing to larger shifts in the deep-UV region, the approach proposed in this study can provide higher sensitivities, and thus more efficient gas detection, than that based on the near-UV LSPR.

LSPR response to different concentrations of ethanol and acetone was examined for two samples to evaluate their sensitivity and detection limit. Figure 5 presents LSPR wavelength shifts induced by ethanol (circles) and acetone (triangles) as a function of gas concentration for samples 4 (red symbols) and 1 (black symbols). The acetone concentrations used for the two samples were limited to 1,500 and 4,000 ppm (triangles in Fig. 5), since strong absorption peaks at 260 and 300 nm influenced the shifts of LSPR peaks in these samples at higher acetone concentrations. The LSPR wavelength shift in the UV range is seen to depend on gas concentration and species, similarly to that previously reported for photonic sensors working in the visible range.[15] It is also seen that the LSPR wavelength shift is larger at higher gas concentrations. Compared with ethanol, acetone gas induces less pronounced shifts, which is believed to be attributed to its high saturated vapor pressure.[15] This was supported by an additional test in which ethanol also demonstrated a small LSPR shift when a minipump was attached to the test chamber to create a low-pressure environment.

Because the slope of all curves in Fig. 5 is seen to decrease gradually at higher concentrations, linear relations are expected below ~1,000 ppm where the inherent sensitivity for UV plasmonic sensing should be evaluated. At 500 ppm of ethanol, the LSPR wavelengths of the two samples observed at 270 and 295 nm are seen in Fig. 5 to shift by 2 and 1 nm, respectively. Correspondingly, the sensitivity, which is defined as $\Delta\lambda/\Delta C$ (nm/ppm), was found to be around 0.004 and 0.002 nm/ppm. Here, $\Delta\lambda$ and ΔC stand for the LSPR wavelength shift and concentration change, respectively. These sensitivity values obtained by us with UV-LSPR detection are one order of magnitude higher than those previously reported for silver nanoprisms with vis-LSPR detection.[15] An enhancement of sensitivity at wavelengths where analyte molecues absorb was previously reported by Zhao et al. for vis-LSPR.[9] Therefore, the higher sensitivity demonstrated by our UV plasmonic device is believed to be attributed to larger refractive-index changes of the ethanol-molecule layer (on the nanoparticle surface) in the deep-UV range.

Considering the error bars observed in Fig. 5 and the wavelength resolution of the spectrometer used in this study (1 nm), the detection limits achieved with the photonic systems developed in this work were 500 and 1,500 ppm for ethanol and acetone, respectively. The instabilities demonstrated by a CCD camera during spectral acquisition in the deep-UV range slightly diminished the accuracy of LSPR observations around 270 nm, which resulted in a detection limit comparable to those achieved at longer LSPR wavelengths. Nevertheless, we believe that higher sensitivities and lower detection limits will be achieved with UV plasmonic systems by improving the sensitivity of detectors and using spectrometry with a higher resolution. Moreover, if nanomate-

rials of less reactive metals (whose surface is purely metallic) and with an LSPR effect in the UV range are prepared, such materials may boost the development of new-generation sensors with much improved sensing performance.

In conclusion, for the first time, sensitive gas detection based on LSPR in the UV range (UV-LSPR) was demonstrated. As proof of the concept, nanostructures of In with different LSPR wavelengths, all in the UV region (270–322 nm), formed via thermal evaporation in vacuum were tested as gas sensing platforms. Exposure to ethanol was found to induce LSPR wavelength shifts, with the best sensitivity detected in the deep-UV range being as high as 0.004 nm/ppm. The obtained results prove that the UV-LSPR effect can be efficiently used for the detection of gas molecules that absorb light in the UV range. Ethanol and acetone gases were detected with the limits of 500 and 1,500 ppm, respectively, which is believed to be further amended with the improvement of both the instruments for UV light measurement and the nanomaterials with UV plasmonic properties. Further developments in this direction will lead to progress not only in UV-LSPR-based gas sensors but also in extremely intense labels for immunoassays and biochemical sensors.

Acknowledgments This research was financially supported by the Japan Society for the Promotion of Science (JSPS) (Grant No. 15K17431) and the Daiwa Anglo-Japanese Foundation (Daiwa Foundation Award 11425/12174).

1) S. Kawata, Appl. Spectrosc. **67**, 117 (2013).
2) J. N. Anker, W. P. Hall, O. Lyandres, N. C. Shah, J. Zhao, and R. P. Van Duyne, Nat. Mater. **7**, 442 (2008).
3) P. L. Stiles, J. A. Dieringer, N. C. Shah, and R. P. Van Duyne, Annu. Rev. Anal. Chem. **1**, 601 (2008).
4) B. Liedberg, C. Nylander, and I. Lunstrom, Sens. Actuators **4**, 299 (1983).
5) R. C. Jorgenson and S. S. Yee, Sens. Actuators B **12**, 213 (1993).
6) A. Huber, S. Demartis, and D. Neri, J. Mol. Recognition **12**, 198 (1999).
7) M. N. Weiss, R. Srivastava, H. Groger, P. Lo, and S. F. Luo, Sens. Actuators A **51**, 211 (1995).
8) D. R. Shankaran, K. V. Gobi, and N. Miura, Sens. Actuators B **121**, 158 (2007).
9) J. Zhao, L. J. Sherry, G. C. Schatz, and R. P. Van Duyne, IEEE J. Sel. Top. Quantum Electron. **14**, 1418 (2008).
10) J. L. Hu, L. Wang, W. P. Cai, Y. Li, H. B. Zeng, L. Q. Zhao, and P. S. Liu, J. Phys. Chem. C **113**, 19039 (2009).
11) J. M. Bingham, J. N. Anker, L. E. Kreno, and R. P. Van Duyne, J. Am. Chem. Soc. **132**, 17358 (2010).
12) L. E. Kreno, J. T. Hupp, and R. P. Van Duyne, Anal. Chem. **82**, 8042 (2010).
13) C. S. Cheng, Y. Q. Chen, and C. J. Lu, Talanta **73**, 358 (2007).
14) Y. Q. Chen and C. J. Lu, Sens. Actuators B **135**, 492 (2009).
15) W. Ma, H. Yang, W. Wang, P. Gao, and J. Yao, Sensors **11**, 8643 (2011).
16) C. Langhammer, M. Schwind, B. Kasemo, and I. Zoric, Nano. Lett. **8**, 1461 (2008).
17) G. H. Chan, J. Zhao, G. C. Schatz, and R. P. Van Duyne, J. Phys. Chem. C **112**, 13958 (2008).
18) Y. Kumamoto, A. Taguchi, M. Honda, K. Watanabe, Y. Saito, and S. Kawata, ACS Photonics **1**, 598 (2014).
19) S. K. Jha, Z. Ahmed, M. Agio, Y. Ekinci, and J. F. Loffler, J. Am. Chem. Soc. **134**, 1966 (2012).
20) M. Honda, Y. Kumamoto, A. Taguchi, Y. Saito, and S. Kawata, Appl. Phys. Lett. **104**, 061108 (2014).
21) I. Tanabe, Y. Y Tanaka, T. Ryoki, K. Watari, T. Goto, M. Kikawada, W. Inami, Y. Kawata, and Y. Ozaki, Proc. SPIE **9926**, 99260K (2016).
22) J. X. Fu, A. Collins, and Y. P. Zhao, J. Phys. Chem. C **112**, 16784 (2008).
23) M. Honda, Y. Kumamoto, A. Taguchi, Y. Saito, and S. Kawata, J. Phys. D **48**, 184006 (2015).
24) J. Henson, J. DiMaria, and R. Paiellar, J. Appl. Phys. **106**, 093111 (2009).
25) C. F. Bohren and D. R. Huffman, *Absorption and Scattering of Light by Small Particles* (Wiley, New York, 1983) p. 342.
26) J. Kim, H. Schoeller, J. Cho, and S. Park, J. Electron. Mater. **37**, 483 (2008).